Crystallization of $Fe_{73.5}Cu_1RE_3Si_{13.5}B_9$ ribbons with RE = Pr, Nd, Gd

2004 J. Phys.: Condens. Matter 16 5555

(http://iopscience.iop.org/0953-8984/16/30/016)

INSTITUTE OF PHYSICS PUBLISHING JOURNAL OF PHYSICS: CONDENSED MATTER

J. Phys.: Condens. Matter **16** (2004) 5555–5568 PII: S0953-8984(04)77423-8

Crystallization of $Fe_{73.5}Cu_1RE_3Si_{13.5}B_9$ ribbons with RE = Pr, Nd, Gd

J-M Le Breton[1,4], **A Zorkovská**[2] **and M Kašiarová**[3]

[1] Groupe de Physique des Matériaux UMR 6634 CNRS—Université de Rouen, Site universitaire du Madrillet, 76801 Saint-Etienne du Rouvray cedex, France
[2] Institute of Physics, Faculty of Science, PJ Šafárik University, Park Angelinum 9, 041 54 Košice, Slovakia
[3] Institute of Materials Research, Slovak Academy of Sciences, Watsonova 47, 043 53 Košice, Slovakia

E-mail: Jean-Marie.LeBreton@univ-rouen.fr

Received 5 March 2004
Published 16 July 2004
Online at stacks.iop.org/JPhysCM/16/5555
doi:10.1088/0953-8984/16/30/016

Abstract

The crystallization process in $Fe_{73.5}Cu_1RE_3Si_{13.5}B_9$ ribbons with RE = Pr, Nd, Gd is investigated using differential scanning calorimetry, x-ray diffraction and Mössbauer spectrometry. The crystallization steps are characterized after both short time (1 h) isothermal annealing in the 350–650 °C range of temperature and long time (24 h) isothermal annealing at 650 and 700 °C. It is found that the crystallization process is the same for the Pr- and Nd-containing ribbons and the crystallization products are α-Fe(Si), Fe_2B and $(Fe, Si)_{23}B_6$. For the Gd-containing sample, the crystallization occurs at a higher temperature, the same crystallization products are formed and Gd-containing phases are detected after 24 h, 700 °C annealing. The nature of the rare earth influences the crystallization kinetics, as the crystallization process for both Pr and Nd ribbons starts at a lower temperature and has a lower activation energy than that of the Gd ribbon, which is comparable to that of the Finemet alloy.

1. Introduction

Nanocrystalline $Fe_{73.5}Cu_1Nb_3Si_{13.5}B_9$ (Finemet) alloys are obtained by annealing melt spun amorphous ribbons, achieving a nanostructure consisting of α-Fe(Si) nanocrystals embedded in a residual Fe–Nb–B amorphous matrix [1, 2]. The excellent soft magnetic properties of these alloys are related to their nanostructure [3]. A Finemet alloy thus exhibits a high saturation flux density and a very attractive combination of soft magnetic properties such as high permeability with high saturation magnetization [4, 5]. This is related to the

[4] Author to whom any correspondence should be addressed.

disappearance of the magnetocrystalline anisotropy on a macroscopic scale and to a very weak magnetostriction [6]. The Cu and Nb additives play a key role in the formation of the nanocrystalline state: Cu multiplies the nucleation centres and Nb inhibits grain growth [7]. The annealing parameters (time, temperature and atmosphere) must be controlled [8] and the nanocrystalline state can be obtained after conventional annealing under vacuum or an Ar atmosphere for typically 1 h at 550 °C.

The magnetic properties of Finemet-type alloys are strongly influenced by the crystallization process and the nature of the crystallized products. Thus, the addition of other elements or substitution for some of the constituents in soft magnetic nanocrystalline Finemet are methods widely used to modify the magnetic properties of the alloy. Slight changes in the chemistry of the initial nominal composition are expected to lead to different crystallization kinetics and can lead to different crystallization products. This is the case for rare earth addition. Indeed, it has been shown that Gd addition changes the microstructure of the nanocrystalline alloy by promoting the formation of Gd–Fe–B ternary phases [9], thus affecting the magnetic properties of the alloy [10, 11]. In addition, the replacement of Nb by a rare earth (Pr, Nd, Gd) can promote the formation of a nanocrystalline structure at an optimum annealing temperature, and results in an increase of the coercivity after annealing at temperatures higher than the optimum temperature [12]. Thus, it appears that the nature of the rare earth influences the magnetic properties of Finemet-type alloys, and this can be related to a modification of the crystallization process. Consequently, the influence of the nature of the rare earth on the crystallization process of Finemet nanocrystalline alloys has still to be investigated. This is the aim of the present investigation.

We present here the results of combined differential scanning calorimetry, x-ray diffraction and Mössbauer spectral studies of the crystallization process of $Fe_{73.5}Cu_1RE_3Si_{13.5}B_9$ ribbons (RE = Pr, Nd, Gd). The influence of the annealing temperature and time are emphasized.

2. Experimental details

Amorphous ribbons of nominal composition $Fe_{73.5}Cu_1RE_3Si_{13.5}B_9$, with RE = Pr, Nd or Gd, were prepared by melt spinning under an inert Ar atmosphere. In the following, the ribbons are denoted as Pr ribbon, Nd ribbon and Gd ribbon, respectively. Annealing treatments were performed at temperatures between 350 and 650 °C for 1 h and at 650 and 700 °C for 24 h in a tubular furnace under a secondary vacuum (10^{-5} Pa) with a continuous pumping, to prevent oxidation. For each treatment, the three ribbons were annealed together, in the same sample holder. The thickness of the ribbons is about 40 μm.

The crystallization kinetics was studied by differential scanning calorimetry (DSC) using a Perkin-Elmer DSC-7 calorimeter at heating rates 4–80 K min^{-1}, in the 100–600 °C temperature range.

X-ray diffraction (XRD) analyses were performed by means of reflection, in an evacuated chamber using a fast curved detector INEL CPS 120. The x-ray generator is equipped with a Co anticathode, using Co Kα radiation ($\lambda = 0.179\,09$ nm). XRD allows one to investigate a surface layer of about 5 μm.

Mössbauer spectral (MS) analyses were performed at room temperature by means of transmission using a ^{57}Co source in a rhodium matrix, the γ-beam direction being perpendicular to the ribbon plane. Transmission MS analysis allows one to analyse the ribbons across their whole thickness. The isomer shift is relative to metallic α-Fe at room temperature. The hyperfine field is denoted as B. Estimated errors for the hyperfine parameters originate from the statistical errors σ given by the fitting program [13], taking 3σ.

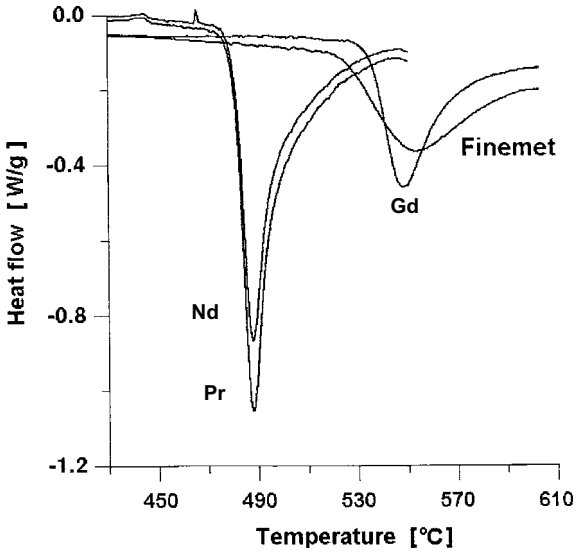

Figure 1. DSC scans of the Pr, Nd, Gd and Finemet ribbons (heating rate 10 K min^{-1}).

3. Results

3.1. Kinetic parameters of the first crystallization process: DSC experiments

In order to characterize the influence of the rare earth on the first crystallization process of the amorphous ribbons, DSC experiments were performed. Typical DSC scans obtained with a 10 K min^{-1} heating rate are shown in figure 1, where they are compared with the DSC scan of a Finemet ribbon performed in the same experimental conditions. The Pr and Nd ribbons show similar behaviours, the maximum of the first exothermic peak being around 490 °C for both samples. For the Gd ribbon, the position of the maximum of the exothermic peak is around 550 °C, very close to that of the Finemet ribbon. This suggests that the Pr and Nd ribbons have very similar crystallization behaviours, different from that of the Gd ribbon.

The kinetic parameters of the first crystallization process (activation energy E, pre-exponential factor K_0 and Avrami exponent n) were calculated for each alloy by means of the Kissinger method, according to the Johnson and Mehl, Avrami and Kolmogorov (JMAK) nucleation-and-growth theory [14], starting from the basic JMAK equation for a constant heating rate:

$$\alpha(T, v) = 1 - \exp[(-K(T)T/v)^n] \qquad \text{with } K(T) = K_0 \exp(-E/RT)$$

where α is the crystallized volume fraction, $K(T)$ the nucleation and growth rate constant, R the gas constant, T the temperature, v the heating rate and n the Avrami exponent. The experimentally obtained dependences of $\ln[\ln(1-\alpha)]$ versus $\ln(T/v) - (E/RT)$, shown in figure 2, are not linear. They can be divided into two linear parts, in such a way that they determine two different Avrami exponents corresponding to the middle and final crystallization stages. In the middle stage the values of n are usually between 2.5 and 4, suggesting a three-dimensional nucleation and growth process. In the final stage, n decreases and approaches a constant value of around 0.7, indicating a strong reduction of both nucleation rate and grain growth [15]. The kinetic parameters obtained are given in table 1.

The values obtained for Pr and Nd ribbons are very close, thus confirming that the first crystallization processes of the Pr and Nd ribbons are similar. K_0 is related to

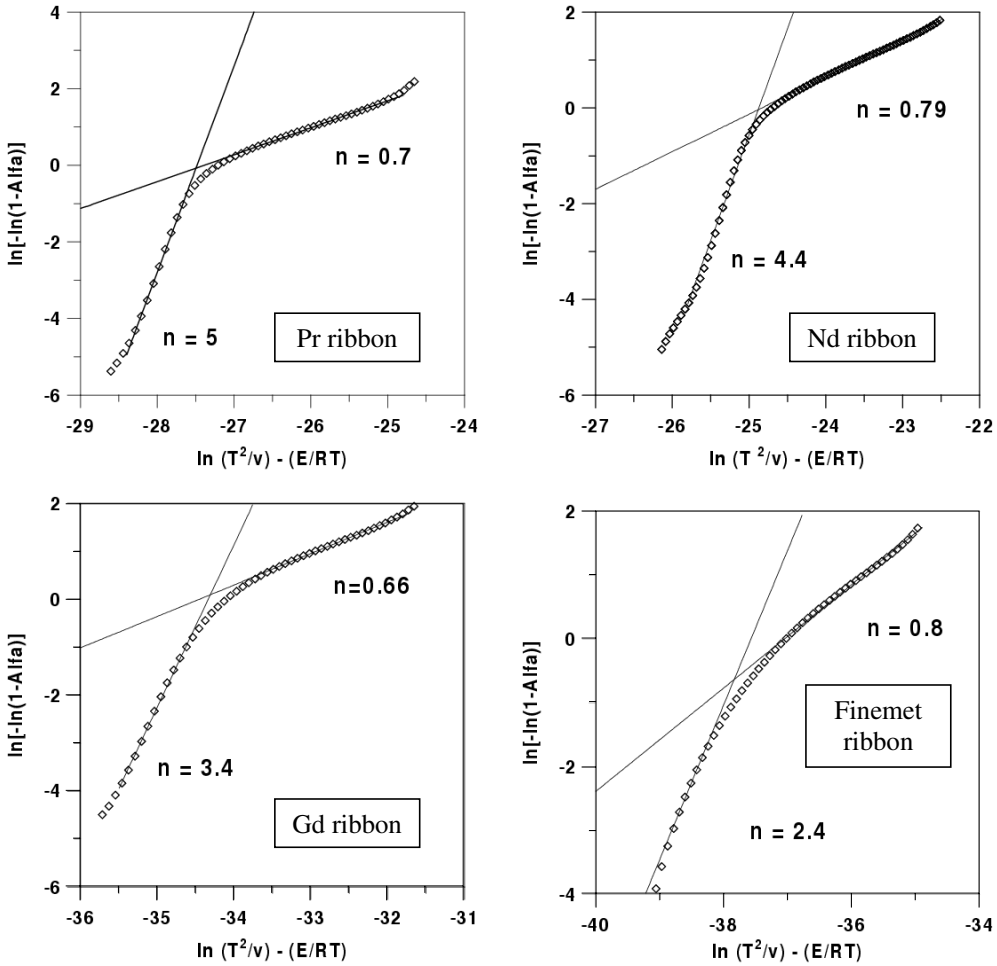

Figure 2. Experimental dependences of $\ln[\ln(1-\alpha)]$ versus $\ln(T/v) - (E/RT)$, for the Pr, Nd, Gd and Finemet ribbons.

Table 1. Kinetic parameters related to the first crystallization step of the amorphous ribbons obtained from the DSC curves according to the JMAK theory.

	Pr ribbon	Nd ribbon	Gd ribbon	Finemet
E (kJ mol^{-1})	269 ± 16	253 ± 13	338 ± 6	359 ± 14
K_0 (s^{-1})	3.0×10^{16}	2.5×10^{15}	3.8×10^{19}	6.4×10^{20}
n (middle stage)	5.0	4.4	3.4	2.4
n (final stage)	0.70	0.79	0.66	0.80

the frequency factor in single-atom processes during normal crystallization, having typical values in the 10^9–10^{14} s^{-1} range, and is higher by several orders of magnitude for a nanocrystallization process. The values of K_0 obtained for the Pr and Nd ribbons are not typical for a nanocrystallization process, especially for the Nd ribbon. This suggests that the nanocrystallization proceeds not only by single-atom processes, but also by more effective ones, such as the cluster-shear mechanism [15]. These results indicate that the microstructure

of the crystallized Pr and Nd ribbons is not as fine as that of a Finemet alloy, for which the grain size is typically 10 nm. This is in agreement with previous transmission electron microscopy observations of Nd ribbons annealed at 425 °C for 1 h, which reveal crystals with grain size between 40 and 100 nm and a small nucleation density [12].

The values obtained for the Gd ribbon are close to those for the Finemet ribbon, indicating that the first crystallization process of the Gd ribbon is similar to that of the Finemet alloy, the values of K_0 being typical for a nanocrystallization process, in agreement with both previous transmission electron microscopy observations [12] and structural investigations of Gd-substituted Finemet alloys [9].

These DSC experiments show that the nature of the rare earth influences the kinetics of the first crystallization process of the ribbons: the crystallization of the Pr and Nd ribbons starts at a lower temperature and has a lower activation energy than the crystallization of the Gd ribbon. Moreover, the first crystallization process of the Gd ribbon is similar to that of the Finemet alloy.

In the following, the crystallization steps and the crystallization products are characterized by XRD and MS analyses after both short time (1 h) isothermal annealing in the 350–650 °C range of temperature and long time (24 h) isothermal annealing at 650 and 700 °C.

3.2. Characterization of the crystallization steps: XRD analysis

The XRD patterns of as-quenched and annealed Pr, Nd and Gd ribbons are shown in figures 3,4 and 5, respectively. The XRD patterns of the as-quenched ribbons display a very broad peak, typical for an amorphous phase. For both Gd and Pr ribbons, the main peak of the α-Fe(Si) phase is observed as well, with a very weak intensity. This is related to the presence of some α-Fe(Si) crystallites located on the surface of the ribbons.

The XRD patterns of the ribbons annealed at 350 and 400 °C are similar to those of the as-quenched ribbons, showing that the corresponding ribbons are still mainly amorphous. It is to be noted that in the case of the Pr ribbon, the intensity of the α-Fe(Si) peak increases, indicating very probably that the surface crystallization process of the ribbon goes on further. After annealing at 450 °C for 1 h, the peaks of α-Fe(Si) drastically increased, due to the crystallization of the ribbons. Additional peaks corresponding to the Fe_3Si phase are observed (at 15.8°, 18.4° and 31.6°), indicating the presence of ordered zones in the α-Fe(Si) phase. The amorphous peak is still observed, indicating that the crystallization process is not terminated. After annealing at 550 °C for 1 h, broad peaks with a weak intensity appear, peaks which are attributed to an Fe–B phase, a precursor of the iron borides. After annealing at 650 °C for 1 h, the pattern of the Gd ribbon displays the same structure as after annealing at 550 °C, showing no evolution of the phase structure in this ribbon. In the patterns of the Nd and Pr ribbons, the peaks of the Fe_2B phase and the main peak of the $(Fe, Si)_{23}B_6$ phase are detected, in relation to the evolution of the Fe–B precursor.

After annealing at 650 and 700 °C for 24 h, the patterns of the Nd and Pr ribbons did not show any additional peak, indicating that no additional phase was formed. The XRD peaks of the α-Fe(Si) phase narrow substantially, indicating the formation of α-Fe(Si) grains with a size that is higher than after annealing at lower temperature. The intensity of the Fe_2B peaks increases, due either to an increase of the size of the Fe_2B grains or to an increase of the crystallinity of the phase. The pattern of the Gd ribbon annealed at 650 °C shows the presence of Fe_2B and $(Fe, Si)_{23}B_6$ peaks, due to the crystallization of the Fe borides. After annealing at 700 °C, additional peaks are detected, that correspond to the body-centred cubic $Gd_3Fe_{62}B_{14}$ metastable phase. This phase has already been observed in $Fe_{68.5}Gd_5Cu_1Nb_3Si_{13.5}B_9$ ribbons annealed at 720 °C for 30 min [9]. The main peak of the Gd_2O_3 oxide phase is observed as well, indicating that the surface of the Gd ribbon is partly oxidized.

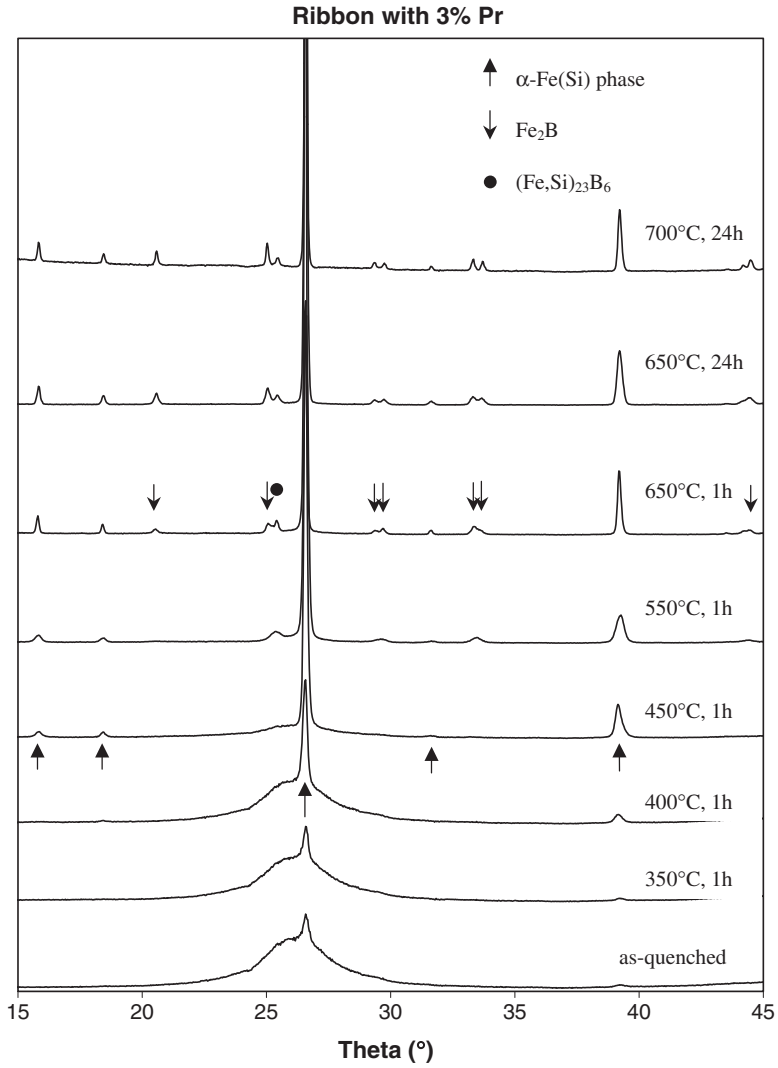

Figure 3. XRD patterns of the as-quenched and annealed $Fe_{73.5}Cu_1Pr_3Si_{13.5}B_9$ ribbons.

As the three ribbons were annealed together at 700 °C for 24 h, the presence of rare earth oxides at the surface of only the Gd ribbon must be related to the crystallization of Gd-containing phases. The rare earth atoms are very probably present in the Fe–B phases, being accommodated by the Fe–B lattices, as already observed in crystallized Sm–Fe–B ribbons [16]. Upon annealing, the Gd atoms are released from the Fe–B phases, to form Gd–Fe–B phases, while some of them are oxidized. In the case of the Pr and Nd ribbons, the rare earth atoms remain in the Fe–B phases, and no oxides are formed.

Short time (1 h) isothermal annealings show that the crystallization process occurs in several steps:

- *First step*: crystallization of α-Fe(Si) around 450 °C.
- *Second step*: formation of an Fe–B phase, the precursor of the iron borides, around 550 °C.

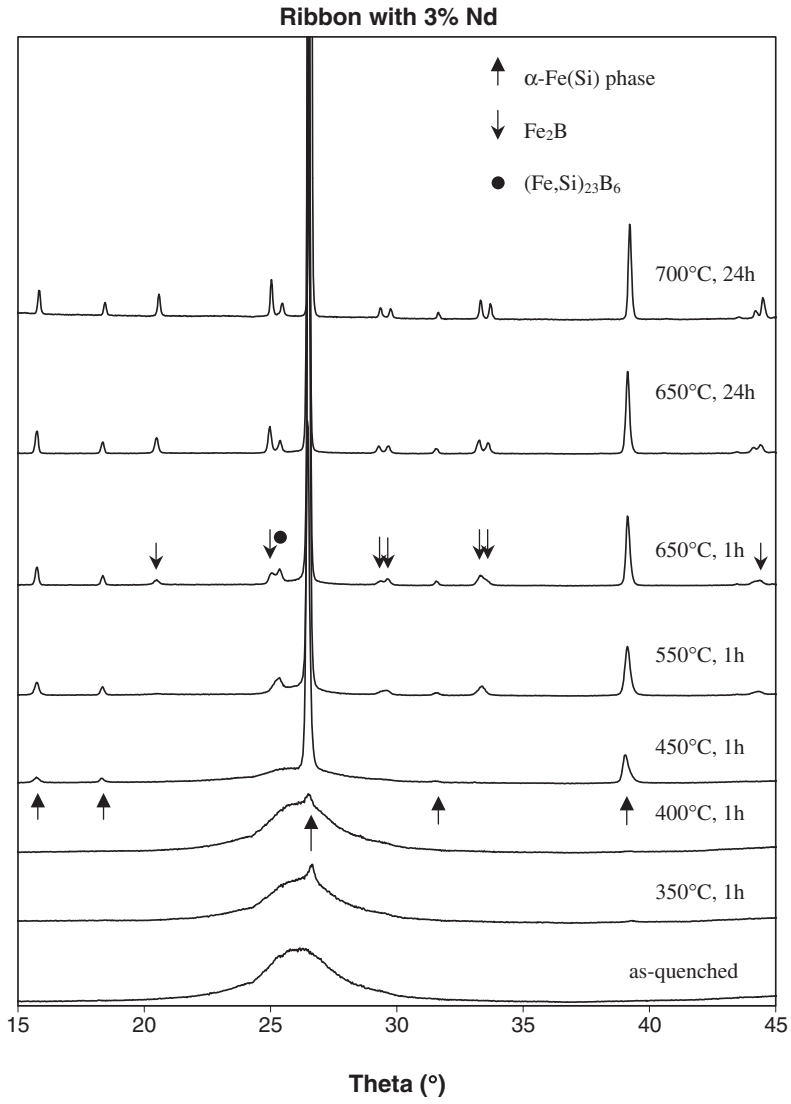

Figure 4. XRD patterns of the as-quenched and annealed $Fe_{73.5}Cu_1Nd_3Si_{13.5}B_9$ ribbons.

- *Third step*: crystallization of Fe_2B and $(Fe, Si)_{23}B_6$ around 650 °C in the case of the Nd and Pr ribbons. This crystallization step is not observed in the case of the Gd ribbon. The third crystallization step is evidenced in the Gd ribbon after long time (24 h) isothermal annealing, showing that it should occur at a temperature higher than 650 °C during short time annealing.
- *Fourth step*: crystallization of RE-containing phases. This is only observed at 700 °C in the case of the Gd ribbon.

The two crystallization stages of the amorphous ribbons characterized by two different Avrami exponents in DSC experiments could thus correspond to the crystallization of the α-Fe(Si) phase and to the crystallization of the Fe–B precursor of the iron borides, respectively.

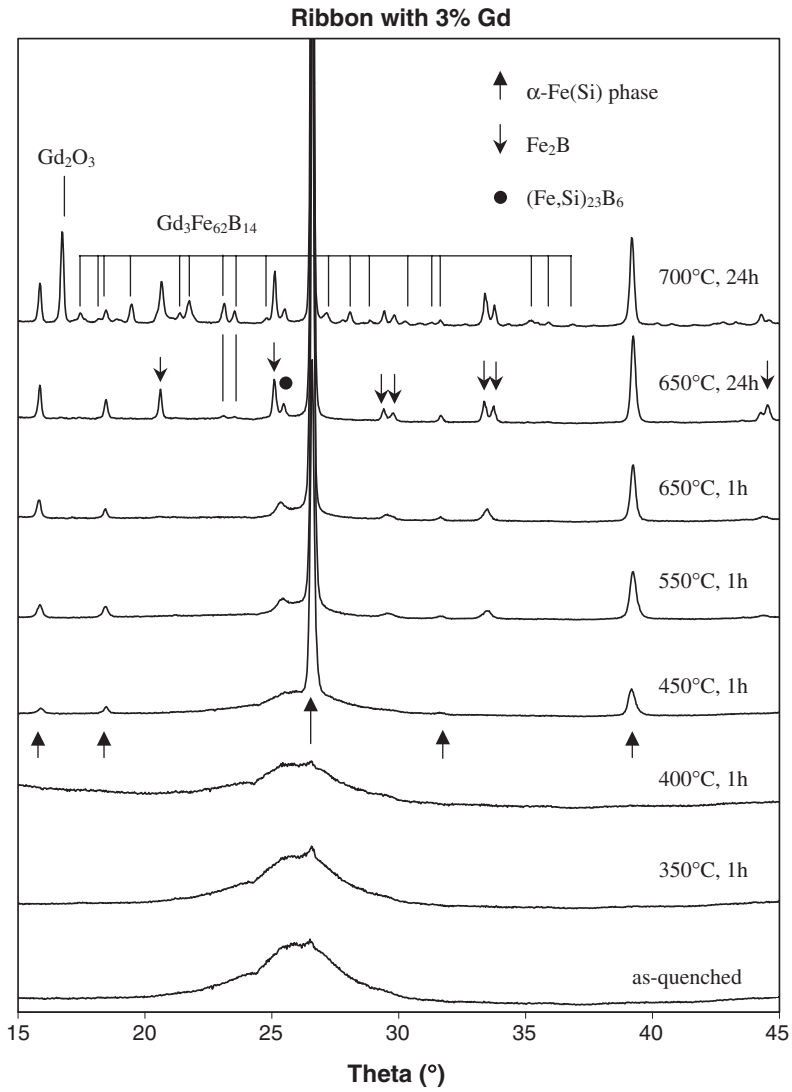

Figure 5. XRD patterns of the as-quenched and annealed $Fe_{73.5}Cu_1Gd_3Si_{13.5}B_9$ ribbons.

3.3. Characterization of the amorphous and crystallized phases: MS analysis

The room temperature Mössbauer spectra of the amorphous and crystallized ribbons are shown in figure 6. A detailed interpretation of the data is presented below. However, general conclusions can be drawn by making a qualitative comparison of the spectra given in the figure. Throughout the whole series, and for each treatment, the Pr and Nd spectra look similar. This indicates that the Pr and Nd annealed ribbons have a similar phase structure, thus confirming that these two ribbons have similar behaviours during the crystallization process.

On the other hand, the Gd spectra show a different behaviour on annealing. In particular, a significant amorphous component is still detected after annealing at 550 °C for 1 h, indicating that the complete crystallization of the Gd ribbon occurs at a higher temperature than that of the Pr and Nd ribbons, in agreement with DSC experiments. Finally, the spectrum of

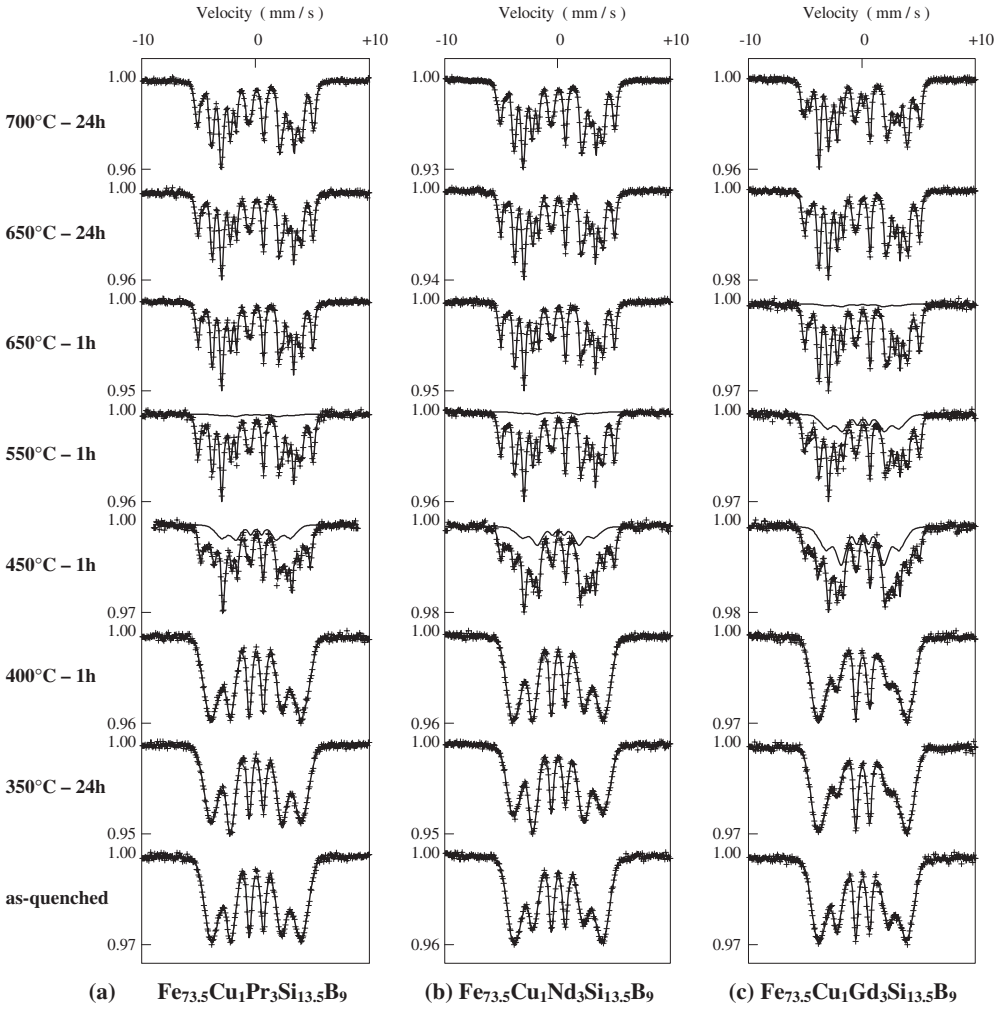

Figure 6. Room temperature Mössbauer spectra of the as-quenched and annealed ribbons. The amorphous component is displayed in the spectra of the ribbons annealed at 450, 550 and 650 °C. The paramagnetic component is displayed in the spectrum of the Gd ribbon annealed at 700 °C.

the Gd ribbon annealed at 700 °C for 24 h shows some differences compared with the other ribbons. These differences are discussed further in the text. This could be related either to the phase transformation of the first crystallization products or to a further crystallization step, in agreement with XRD results.

3.3.1. Characterization of the amorphous phases. After annealing at 350 and 400 °C for 1 h, the Mössbauer spectra of all the ribbons are typical of amorphous samples, showing that the ribbons are still amorphous in volume. This indicates that the α-Fe(Si) phase detected by XRD analysis is located on the surface of the Pr and Gd ribbons. The contribution of the amorphous phase was computer fitted by a least-squares technique [13], using the histogram method relative to a discrete distribution of single crystals [17], and constraining the linewidths of each of the elementary sextets to be the same (0.38 mm s^{-1}). Because of the topological

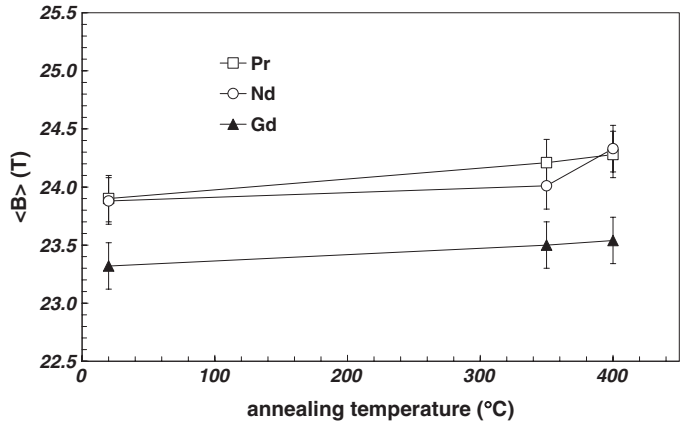

Figure 7. The average hyperfine field $\langle B \rangle$ of the amorphous component in the Mössbauer spectra of as-quenched and annealed Pr, Nd and Gd ribbons.

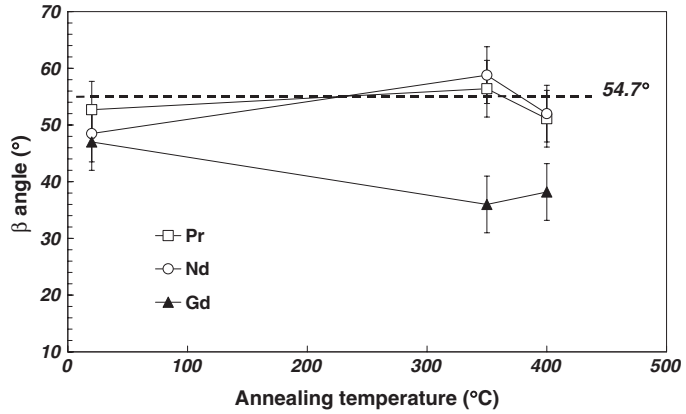

Figure 8. The average angle β of the amorphous component in the Mössbauer spectra of as-quenched and annealed Pr, Nd and Gd ribbons.

disorder, we assumed the mean quadrupolar shift to be zero. The relative intensities of the sextet lines depend on the mean Mössbauer angle β between the incident γ-beam direction and the hyperfine field B. The ratios of the lines vary as $3{:}y{:}1{:}1{:}y{:}3$ with y expressed as $y = \frac{4\sin^2\beta}{1+\cos^2\beta}$.

The average hyperfine field of the amorphous phase is calculated as $\langle B \rangle = \frac{\sum_i P(B_i)B_i}{\sum_i P(B_i)}$, where B_i is the hyperfine field of sextet number i and $P(B_i)$ the corresponding relative area. As shown in figure 7, $\langle B \rangle$ is higher for the Pr and Nd ribbons than for the Gd ribbon, in agreement with magnetic measurements [12]. A slight increase of the average hyperfine field is observed for all the samples upon annealing (figure 7). This is attributed to structural modifications in the amorphous phase, related to slight changes of the environments around the Fe atoms.

In the case of the as-quenched ribbons, the Mössbauer angle β (the angle between the incident γ-beam direction and the direction of the Fe moment) is slightly below 54.7° (figure 8). This value corresponds to a random distribution of the directions of the Fe moments in the

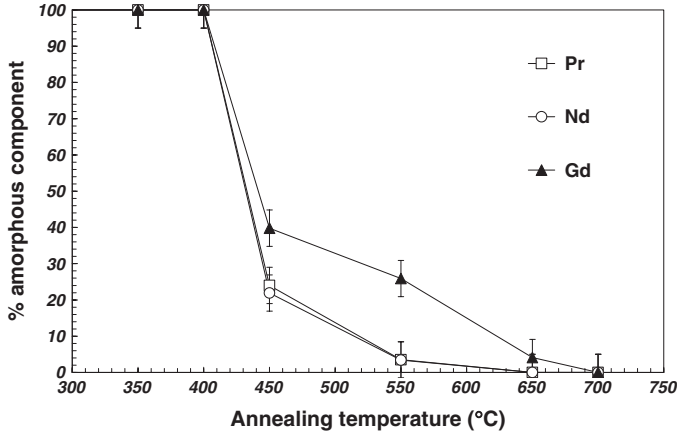

Figure 9. The relative intensity of the amorphous component obtained from the fitting of the Mössbauer spectra.

ribbon. No significant change is observed on annealing for the Pr and Nd ribbons. For the Gd ribbon, the value tends to 37° after annealing, which indicates that the Fe moments have a tendency to rotate towards the normal to the ribbon plane.

The evolution with the annealing temperature of the relative area of the amorphous component is shown in figure 9. It can be seen that between 450 and 650 °C, the areas of the amorphous components in the Pr and Nd ribbons are the same, in agreement with the fact that the crystallizations of these ribbons occur at the same temperature. On the other hand, the area of the amorphous component in the Gd ribbon is higher than in the Pr and Nd ribbons, in agreement with the fact that the temperature of the first crystallization step in the Gd ribbon is higher than those for the other ribbons.

3.3.2. Characterization of the crystallized phases. The Mössbauer spectra of the ribbons annealed at temperatures higher than 450 °C were fitted in agreement with the results of XRD analysis. It is to be noted that all the spectra were fitted consistently, with the same fitting procedure, described hereafter. According to the literature [18], the Mössbauer spectrum of the α-Fe(Si) phase can be fitted with four, five or six sextets, corresponding to the different environments around the Fe atoms in the bcc unit cell. On the other hand, the hyperfine parameters of the contributions of the Fe–B phases (Fe_2B, $Fe_{23}B_6$, Fe_3B) are very close to those of some of the α-Fe(Si) contributions. Consequently, and because the boride phases are present in small amounts in the samples, their contributions were considered together with that of the α-Fe(Si) phase in a so-called 'crystalline fraction', that was fitted with eight sextets. This fitting procedure allows one to obtain very satisfactory fittings (figure 6). The results show that some sextets have very close hyperfine fields. So the corresponding sextets were considered together in a same contribution, and five contributions were considered, each contribution containing one, two or three sextets. An example is given in figure 10.

The five contributions of the crystalline fraction were fitted in the spectra of the ribbons annealed at temperature higher than 450 °C. For the Pr and Nd ribbons, the corresponding histograms are very similar, no significant difference being observed. Some typical distributions are shown in figure 11 for the Nd ribbon. This means that the crystallized phases that contain Fe are present in the same proportions. The $P(B)$ distributions for the Nd ribbons annealed between 550 and 700 °C are similar (see figure 11), indicating that there is no evolution of the crystalline fraction on annealing.

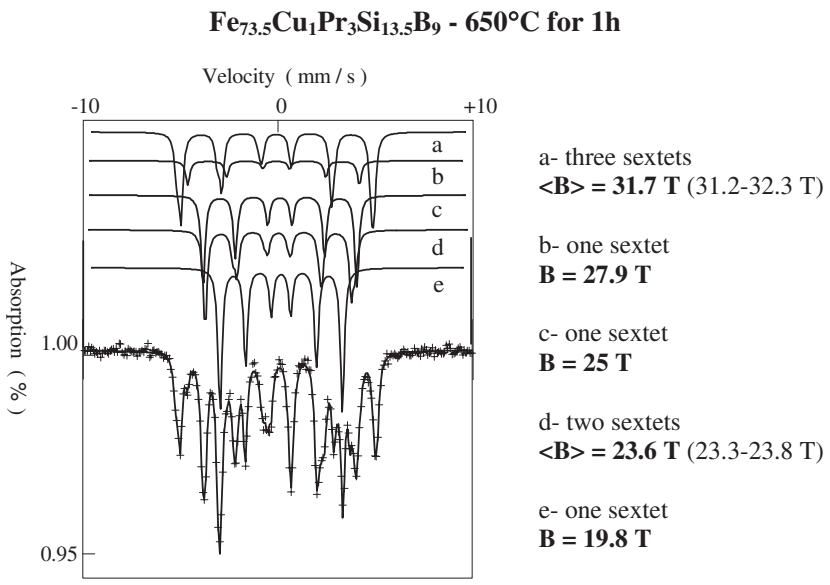

Figure 10. The room temperature Mössbauer spectrum of the $Fe_{73.5}Cu_1Pr_3Si_{13.5}B_9$ ribbon annealed at 650 °C for 1 h. The five contributions to the spectrum are displayed (in (a) and (d), the contribution shown is the sum of the sextets that have close hyperfine fields).

After annealing at 700 °C for 24 h, a significant evolution of the Mössbauer spectrum of the Gd ribbon is observed (figure 6). First, a paramagnetic component is fitted at the centre of the spectrum (isomer shift: 0.20 mm s^{-1}; relative area: 2%), as displayed in figure 6(c). Second, a change in the $P(B)$ distribution is observed, with a decrease of the contribution with $B = 19.7$ T and an increase of the contributions with $\langle B \rangle = 23.6$ and 31.0 T (see figure 11). The increase of the contribution with $\langle B \rangle = 23.6$ T must be related to the crystallization of the metastable $Gd_3Fe_{62}B_{14}$ phase, whose Mössbauer contribution consists mainly of a magnetic sextet with a hyperfine field of about 23 T [9]. According to its high Fe content, the formation of the $Gd_3Fe_{62}B_{14}$ phase results in a decrease of the relative area of the contribution of the Fe–B phases, corresponding to the decrease of the contribution with $B = 19.7$ T. On the other hand, it is known that the metastable $Gd_3Fe_{62}B_{14}$ phase transforms into α-Fe and $Gd_{1.1}Fe_4B_4$ phases upon annealing [9]. The decomposition of the $Gd_3Fe_{62}B_{14}$ phase may thus be responsible for both the increase of the contribution with $\langle B \rangle = 31.0$ T (through the formation of α-Fe, with $B = 33.0$ T) and the appearance of the paramagnetic component (through the formation of the paramagnetic $Gd_{1.1}Fe_4B_4$ phase).

The results of the Mössbauer investigation confirm the results of both DSC experiments and XRD analyses. The crystallization of the amorphous phase occurs by the same process in the three ribbons, but with different kinetics. The complete crystallization of the Gd ribbon occurs at a higher temperature than that of the Pr and Nd ribbons, and Gd-containing phases are detected after annealing at 700 °C for 24 h.

4. Conclusion

The crystallization process in $Fe_{73.5}Cu_1RE_3Si_{13.5}B_9$ ribbons with RE = Pr, Nd, Gd has been investigated using differential scanning calorimetry, x-ray diffraction and Mössbauer spectrometry. The crystallization steps and the crystallization products have been characterized

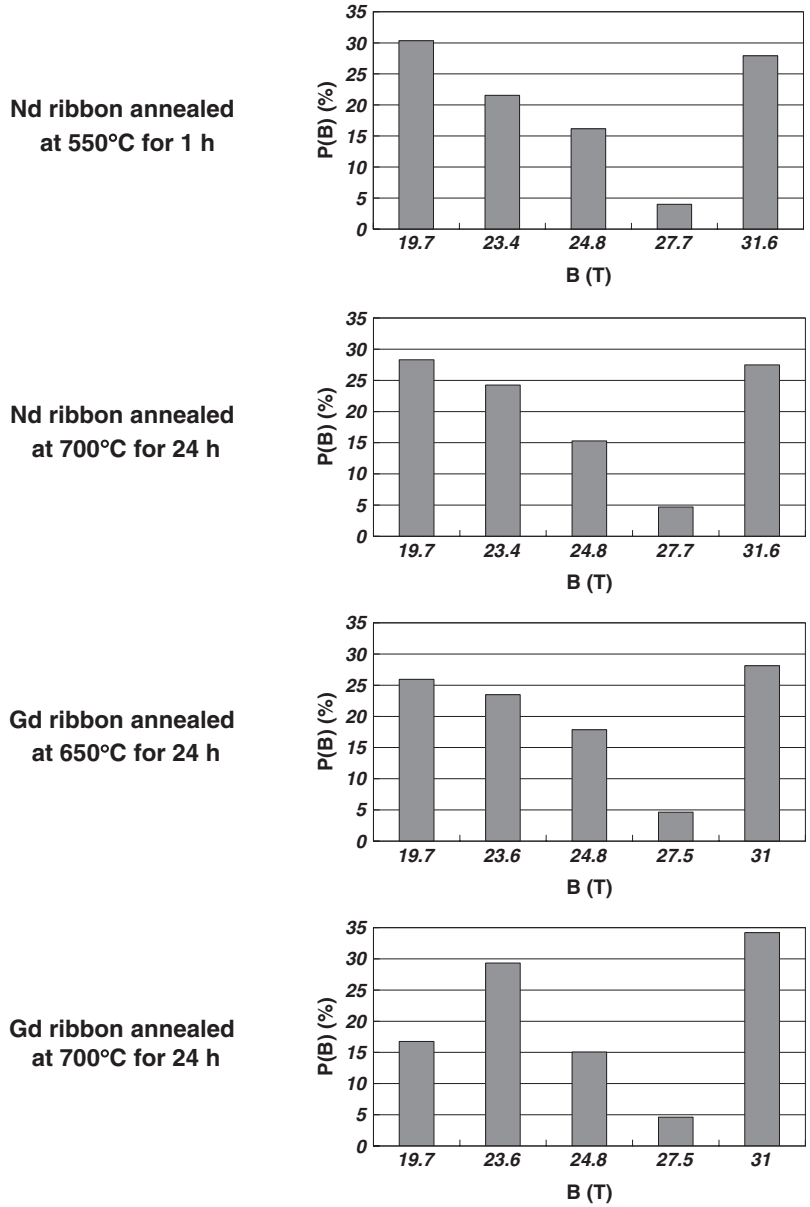

Figure 11. Histograms corresponding to the crystalline fraction fitted in the spectra of the annealed ribbons for the treatments indicated.

after both short time (1 h) isothermal annealing in the 350–650 °C range of temperature and long time (24 h) isothermal annealing at 650 and 700 °C. The results show that the crystallization process occurs in several steps:

(i) crystallization of α-Fe(Si),
(ii) formation of the Fe–B precursor of the iron borides,
(iii) crystallization of Fe_2B and $(Fe, Si)_{23}B_6$,
(iv) crystallization of RE-containing phases.

For the annealing conditions investigated here, the RE-containing phases were only observed in the case of the Gd ribbon.

This investigation shows that the nature of the rare earth influences the kinetics of the crystallization process. The first crystallization process of the Gd ribbon is similar to that of the Finemet alloy. The crystallization processes of the Pr and Nd ribbons, which are similar, start at a lower temperature and have a lower activation energy than that of the Finemet alloy.

References

[1] Yoshizawa Y, Oguma S and Yamauchi K 1998 *J. Appl. Phys.* **64** 6044
[2] Herzer G 1989 *IEEE Trans. Magn.* **25** 3327
[3] Crisan O, Grenèche J M, Le Breton J M, Crisan A D, Labaye Y, Berger L and Filoti G 2003 *Eur. Phys. J.* B **34** 155
[4] Yoshizawa Y and Yamauchi K 1991 *Mater. Sci. Eng.* A **133** 176
[5] He K Y 1996 *Proc. Ist Int. Symp. on Magnetic Industry* vol 3, ed F-Z Lian and Q L Hu to be published
[6] Herzer G 1992 *J. Magn. Magn. Mater.* **112** 258
[7] Hono K, Hiraga K, Wang Q, Inoue A and Sakurai T 1992 *Acta Metall. Mater.* **40** 2137
[8] Grognet S, Le Breton J M, Atmani H and Teillet J 2000 *J. Magn. Magn. Mater.* **210** 167
[9] Crisan O, Le Breton J M, Jianu A, Teillet J and Filoti G 1997 *J. Alloys Compounds* **262/263** 381
[10] Crisan O, Le Breton J M, Noguès M, Machizaud F, Jianu A, Teillet J and Filoti G 1998 *J. Physique* IV **8** 2–115
[11] Crisan O, Le Breton J M, Crisan A D and Machizaud F 2004 *J. Magn. Magn. Mater.* **272–276** 1396
[12] Zorkovská A, Kollár P, Kováč J, Sovák P, Matta P and Konč M 1998 *J. Physique* IV **8** 2–237
[13] Teillet J and Varret F 1983 *MOSFIT Program* unpublished
[14] Kissinger H E 1957 *Anal. Chem.* **29** 1702
[15] Lu K 1996 *Mater. Sci. Eng.* R **16** 161
[16] Crisan O, Le Breton J M, Noguès M, Machizaud F and Filoti G 2002 *J. Phys.: Condens. Matter* **14** 12599
[17] Varret F 1982 *Proc. Int. Conf. on the Applications of the Mössbauer Effect* (New Delhi: Indian National Science Academy) p 129
[18] Grenèche J M 1997 *Hyperfine Interact.* **110** 1 and references therein